Inorganic Chemistry

pubs.acs.org/IC Article

Enhanced Electrochemical CO_2 Reduction by a Series of Molecular Rhenium Catalysts Decorated with Second-Sphere Hydrogen-Bond Donors

Kallol Talukdar,[†] Sayontani Sinha Roy,[†] Eva Amatya, Elizabeth A. Sleeper, Pierre Le Magueres, and Jonah W. Jurss*

Cite This: https://dx.doi.org/10.1021/acs.inorgchem.0c00154 Read Online

ABSTRACT: A series of rhenium(I) *fac*-tricarbonyl complexes containing pendent arylamine functionality in the second coordination sphere have been developed and studied as electrocatalysts for carbon dioxide (CO_2) reduction. Aniline moieties were appended at the 6 position of a 2,2′-bipyridine (bpy) donor in which the primary amine was positioned at the *ortho-* (**1-Re**), *meta-* (**2-Re**), and *para-* (**3-Re**) sites of the aniline substituent to generate a family of isomers. The relationship between the catalyst structure and activity was explored across the series, and the catalytic performance was compared to that of the benchmark catalyst $Re(bpy)(CO)_3Cl$ (**ReBpy**). Catalysts **1-Re**, **2-Re**, and **3-Re** outperform the benchmark catalyst both in anhydrous acetonitrile and with added trifluoroethanol (TFE) as an external proton source. In the presence of TFE, the aniline-substituted catalysts convert CO_2 to carbon monoxide (CO) with high Faradaic efficiencies (≥89%) and have superior turnover frequencies (TOFs) relative to **ReBpy** (72.9 s^{-1}), with **2-Re** having the highest TOF of the series at 239 s^{-1}, a value that is twice that of the next most active catalyst. TOFs of 123 and 109 s^{-1} were observed for the *ortho-* and *para*-substituted aniline complexes (**1-Re** and **3-Re**), respectively. Indeed, catalytic activities vary widely across the series, showing a high sensitivity to the position of the amine functionality relative to the rhenium active site. IR and UV−vis spectroelectrochemical experiments were conducted on the aniline-substituted systems, revealing important differences between the catalysts and mechanistic insight.

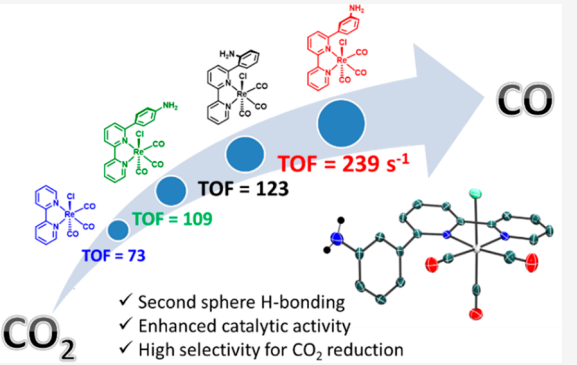

INTRODUCTION

Global energy consumption continues to increase with ∼80% of this energy sourced from nonrenewable fossil fuels. The combustion of fossil fuels releases airborne pollutants and copious amounts of carbon dioxide (CO_2) into the atmosphere, which has contributed to climate change and other environmental problems.[1−3] Indeed, CO_2 is a greenhouse gas whose atmospheric concentration has risen to levels not seen in at least 800,000 years.[4] Renewable energy sources offer a clean alternative to fossil fuels, but they are intermittent and geographically diffuse. Thus, energy storage is required to power society night and day and to meet the energy demands of dense population centers. To address this challenge, renewable electricity can be converted into chemical energy by reducing CO_2 into energy-rich fuels (or fuel precursors) as part of a closed carbon cycle.[5,6] However, large overpotentials are often required to overcome activation barriers for CO_2 conversion, and more efficient catalysts are needed to effectively reduce CO_2 into value-added products.

The direct one-electron reduction of CO_2 to the highly energetic $CO_2^{\bullet-}$ radical anion can be circumvented with catalysts capable of mediating lower-energy multielectron/multiproton processes. However, product selectivity is also required in the presence of a proton source where hydrogen evolution is often a competing side reaction that reduces efficiency.[7] The development of well-defined homogeneous electrocatalysts for reducing CO_2 at a low overpotential and with high product selectivity is still a significant scientific challenge.[5,8,9]

Nature achieves catalytic reactions with high efficiency and selectivity by employing tightly regulated environments within metalloenzymes. Metalloenzymes such as Ni,Fe-carbon monoxide dehydrogenase[10] and formic acid dehydrogenase[11] are known to efficiently catalyze CO_2 reduction to carbon monoxide (CO) or formate through cooperative bimetallic CO_2 activation and/or by stabilization of a metal carboxylate

Received: January 16, 2020

https://dx.doi.org/10.1021/acs.inorgchem.0c00154
Inorg. Chem. XXXX, XXX, XXX−XXX

intermediate with optimally positioned amino acid residues in the second coordination sphere of the active site. Noncovalent second-coordination-sphere interactions are recognized for their importance in directing multielectron/multiproton catalysis.[6,12] Synthetically, noncovalent interactions are difficult to harness in a reliable manner, often causing unwanted structures and perturbation of function.[13−15] Significant effort continues to be exerted by the scientific community to append second-sphere functionality onto the ligand framework of catalysts to provide specific and reproducible intramolecular interactions to improve catalyst performance. Inspired by nature, a variety of synthetic systems have been developed with different functional groups in the secondary coordination sphere of the catalytic active site.[12] Iron porphyrin complexes decorated with phenolic[16] or quaternary ammonium[17] groups are prototypical examples that have dramatically improved the performance metrics for electrocatalytic CO_2 reduction relative to the parent catalyst, both thermodynamically and kinetically.

From their inception, *fac*-Re(bpy)$(CO)_3$Cl (**ReBpy**) catalysts have gained considerable attention due to their exceptional selectivity toward CO_2 reduction over proton reduction.[18−20] Efforts have been made to enhance the activity of this class of catalysts by incorporating thiourea,[21] imidazolium,[22] hydroxyl,[23] and amine[24] functionalities as well as variable peptide linkages[25] into the second coordination sphere. We note that bimetallic complexes with well-defined distances between Re(bpy) units have also been synthesized to access cooperative modes of CO_2 activation and/or to accumulate multiple reducing equivalents to enhance the multielectron reduction of CO_2.[26−28]

In this work, we sought to investigate the effect of pendant aniline groups on catalytic CO_2 reduction in a series of substituted Re(bpy)$(CO)_3$Cl compounds (Figure 1). By

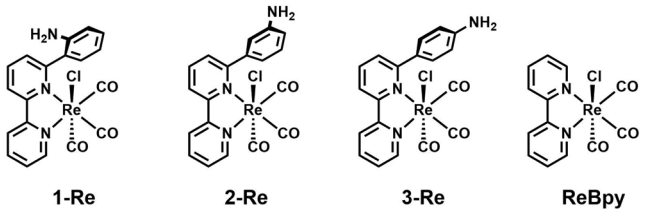

Figure 1. Structures of the catalysts studied in this work.

systematically altering the position of the primary amine on the aniline moiety at the 6 position of each 2,2′-bipyridine donor, we have developed a series of positional isomers to correlate the reactivity of each catalyst with the distance between the pendant amine and rhenium active site.

RESULTS AND DISCUSSION

Synthesis and Structure of the Complexes. Ligands **L1**−**L3** were prepared via palladium-catalyzed Suzuki cross-coupling of 6-bromo-2,2′-bipyridine and the appropriate boronic acid or boronate ester with good-to-excellent yields (Figure 2).[26,29] In all cases, pure products were obtained by silica gel chromatography. Metalation was achieved by refluxing the ligands with 1 equiv of the metal precursor $Re(CO)_5Cl$ in anhydrous toluene for 12 h under a N_2 atmosphere.[26,30] The complexes were purified by washing them with low-polarity organic solvents. Detailed synthetic procedures are described in the Supporting Information (SI). All three complexes are air- and moisture-stable in the solid state. The ligands and complexes were characterized by elemental analysis, ^{1}H NMR, and high-resolution mass spectrometry.

Crystals of **1-Re** and **2-Re** in the form of small yellow needles were grown from slow ether diffusion into a concentrated solution of each complex in acetonitrile (CH_3CN) or *N*,*N*-dimethylformamide (DMF) at low temperature. Several attempts to grow X-ray-quality crystals of **3-Re** were unsuccessful. In theory, a pair of conformers could form during the synthesis of both **1-Re** and **2-Re**. However, only one isomer (amine *syn* to the chloro ligand) was observed in each case by room temperature ^{1}H NMR and from the solid-state crystal structures. This may be credited to electrostatic interactions, the steric demand of the aniline moieties, and hindered rotation around the C−C bond of the pendant aminophenyl group and central pyridine ring. Interestingly, similar rhenium bipyridyl complexes with *o*-methoxyphenyl or *o*-benzoic acid rings at the 6 position of the bipyridine ligand produced the *anti* isomer, where the functional group is oriented away from the chloride donor.[31,32] Thermal ellipsoid plots of **1-Re** and **2-Re** are shown in Figure 3, and selected bond lengths and angles are reported in Table 1.

Both structures depict slightly distorted octahedral geometries around the rhenium(I) center with three carbonyls in a facial arrangement, a κ^2 bipyridyl ligand, and an anionic chloro donor. In **1-Re**, the dihedral angle between the aminophenyl ring and adjacent pyridyl ring is 74.25°. The dihedral angle (64.58°) of **2-Re** is smaller, as expected given the reduced steric demand of this isomer, and similar to the dihedral angle (68.53°) of a related complex containing an unsubstituted phenyl group at the 6 position of 2,2′-bipyridine.[33]

The Re−N2 bond distances in both **1-Re** and **2-Re** are 0.055 Å longer than that of the adjacent, unsubstituted rhenium−pyridine bond distance (Re−N1) due to the steric bulk imposed by the aniline substituents. Unlike **ReBpy**, the bipyridine units in **1-Re** and **2-Re** are not coplanar with the $Re(CO)_2$ plane formed by the *trans*-carbonyl donors.[34]

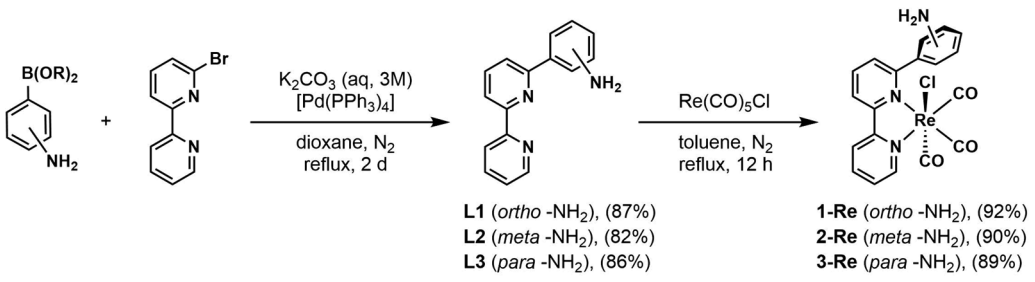

Figure 2. Synthesis of isomeric aniline-substituted bipyridine ligands and their corresponding rhenium tricarbonyl compounds.

https://dx.doi.org/10.1021/acs.inorgchem.0c00154
Inorg. Chem. XXXX, XXX, XXX−XXX

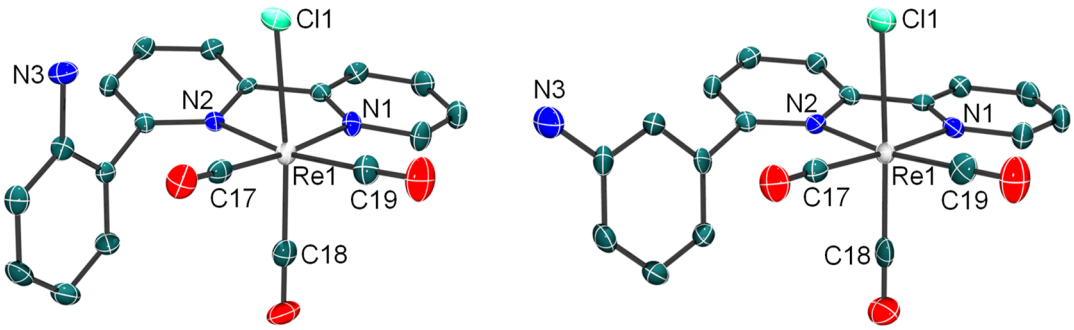

Figure 3. Crystal structures of **1-Re** (left) and **2-Re** (right) with thermal ellipsoids rendered at the 50 and 70% probability levels, respectively. Hydrogen atoms and outer-sphere solvent molecules have been omitted for clarity.

Table 1. Selected Bond Distances and Angles of 1-Re, 2-Re, and ReBpy

selected bond distances[a] and angles	1-Re	2-Re	ReBpy[34]
Re1−N1	2.162(3)	2.166(2)	2.173(6)
Re1−N2	2.217(4)	2.221(2)	2.176(6)
Re1−C17	1.932(4)	1.940(3)	1.932(7)
Re1−C18	1.907(6)	1.920(2)	1.938(9)
Re1−C19	1.900(5)	1.899(3)	1.919(7)
Re1−Cl1	2.490(1)	2.4733(6)	2.460(2)
N1−Re1−N2	74.6(1)	75.09(7)	74.9(2)
dihedral angle[b]	74.25	64.58	
torsion angle[c]	−10.6(6)	−9.6(3)	0.1(8)

[a]All bond distances are reported in angstroms (Å). [b]Dihedral angle between the aminophenyl ring and adjacent pyridyl ring. [c]Torsion angle between the pyridine rings.

Torsion angles of −10.6(6)° and −9.6(3)° between the pyridine rings of **1-Re** and **2-Re**, respectively, are also observed. The Re−Cl bond length is shorter in **2-Re** than in **1-Re**, but both have slightly longer Re−Cl bonds relative to the unsubstituted **ReBpy** complex. The distances between the pendant amine nitrogen atom and the chloro ligand are 3.989(4) and 6.412(2) Å for **1-Re** and **2-Re**, respectively.

Electrochemical Studies under N_2. To assess the redox behavior of the complexes under noncatalytic conditions, cyclic voltammetry was performed in N_2-saturated anhydrous CH_3CN solutions containing a 0.5 mM complex and 0.1 M Bu_4NPF_6 as the supporting electrolyte (Figure 4). All reported potentials are referenced versus the ferrocenium/ferrocene ($Fc^{+/0}$) redox couple.

As observed with **ReBpy**, the three aniline-substituted isomers show a quasi-reversible one-electron-reduction event, followed by a more negative irreversible one-electron reduction in the potential window studied. The reduction potentials and diffusion coefficients of each complex are summarized in Table 2. On the basis of previous reports on **ReBpy**-type

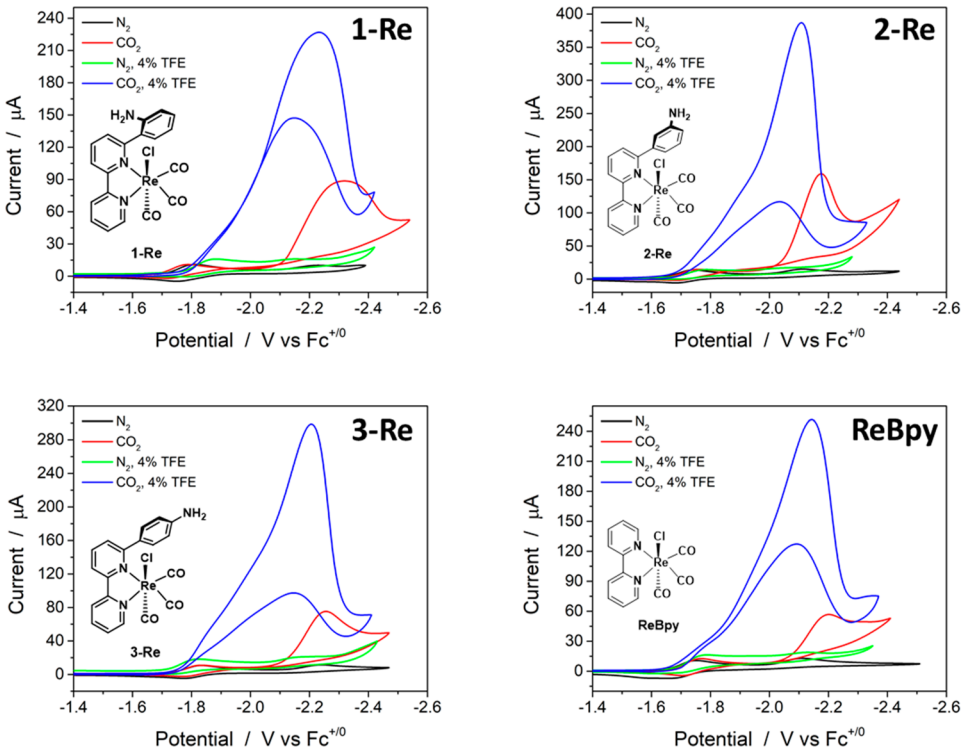

Figure 4. CVs of **1-Re**, **2-Re**, **3-Re**, and **ReBpy** at 0.5 mM concentrations in CH_3CN/0.1 M Bu_4NPF_6 under N_2 (black), CO_2 (red), N_2 with 4% TFE (green), and CO_2 with 4% TFE (blue). Scan rate = 100 mV s^{-1}; glassy carbon working electrode.

https://dx.doi.org/10.1021/acs.inorgchem.0c00154
Inorg. Chem. XXXX, XXX, XXX−XXX

Table 2. Reductive Peak Potentials[a] and Diffusion Coefficients (D) of 1-Re, 2-Re, 3-Re, and ReBpy from Cyclic Voltammetry of a 0.5 mM Complex in Anhydrous CH_3CN/0.1 M Bu_4NPF_6 Solutions under a N_2 Atmosphere[b]

catalyst	$E_{p1,c}$ (V)	$E_{p2,c}$ (V)	D (cm^2 s^{-1})
1-Re	−1.81	−2.22	1.31×10^{-5}
2-Re	−1.73	−2.14	1.18×10^{-5}
3-Re	−1.84	−2.24	1.36×10^{-5}
ReBpy	−1.79	−2.15	1.72×10^{-5}

[a]Potentials are versus $Fc^{+/0}$, rounded to the nearest 0.01 V, and measured at ν = 100 mV s^{-1}. [b]Glassy carbon disk working, platinum wire counter, and silver wire quasi-reference electrodes.

complexes,[18,35] the first reduction is bipyridine-based and forms an anionic ligand-centered radical species, $[Re^{I}(bpy^{\bullet-})(CO)_3Cl]^-$ (where bpy is used generically to encompass the substituted bipyridyl ligands). This species can undergo slow chloride loss through a ligand-to-metal charge transfer, in which the six-coordinate bipyridine π-radical species is favored over the neutral five-coordinate rhenium-centered radical species,[36] or by rapid dissociation of Cl^- at the second reduction. The second irreversible process is assigned to a mostly metal-based reduction (Re^I to Re^0), resulting in a five-coordinate anionic species that is best described as $[Re^0(bpy^{\bullet-})(CO)_3]^-$, which can activate CO_2.[37,38] These assignments are supported by infrared spectroelectrochemical (IR-SEC) experiments (*vide infra*).

The first reduction ($E_{p1,c}$) of the complexes varies by 110 mV. Similar reduction potentials for **1-Re** and **ReBpy** are observed for this process at −1.81 and −1.79 V versus $Fc^{+/0}$, respectively, while **3-Re** has the most cathodic initial reduction at −1.84 V. Complex **2-Re** has the most positive initial reduction of the series (80, 110, and 60 mV more positive than **1-Re**, **3-Re**, and **ReBpy**, respectively) at −1.73 V. The metal-centered reductions of **2-Re** and **ReBpy** occur at very similar potentials, whereas $E_{p2,c}$ of **1-Re** and **3-Re** are 70 and 90 mV more negative than the parent **ReBpy** complex, respectively. The *meta*-substituted aminophenyl group clearly has the smallest electronic effect on the complex, resulting in minor changes in the reduction potentials relative to the parent complex. In contrast and consistent with resonance arguments, the *ortho*- and *para*-substituted aminophenyl groups provide additional electron density to the ligand framework through a resonance-donating effect and are responsible for the cathodically shifted reduction potentials.

The return scan of each complex is relatively complicated due to possible dimer formation/cleavage, chloride dissociation, and solvent coordination.[39−41] For **1-Re**, only one oxidation peak at −1.74 V corresponding to the first reduction is observed in the return scan at 0.1 V s^{-1}. At the same scan rate, **2-Re** shows a prominent oxidation peak at −1.69 V and a smaller feature at −1.56 V; **3-Re** exhibits similar behavior with a prominent peak at −1.76 V and a smaller feature at −1.65 V. The resolution between these two peaks becomes more conspicuous at faster scan rates (Figures S13−S15). Indeed, **1-Re** begins to show an analogous oxidation at −1.6 V, appearing as a shoulder on the prominent peak, at a scan rate of 1 V s^{-1}.

In contrast, upon isolation of the first reduction event, only one reversible oxidation peak is observed at around −1.7 V for all three complexes, which is assigned to the oxidation of one-electron-reduced species $[Re^{I}(bpy^{\bullet-})(CO)_3Cl]^-$.[35,42,43] The potential of this oxidation is analogous to that of the prominent oxidation wave discussed above upon cycling through both reductions, where the redox couple becomes less reversible. The smaller oxidation feature paired with the prominent peak only appears, on this time scale, when cycling through the second reduction. This observation is in agreement with earlier electrochemical experiments on **ReBpy**-type complexes, and thus the less prominent wave of each complex is tentatively assigned to the oxidation of $[Re^0(bpy^{\bullet-})(CO)_3]^-$.[39,40]

At more positive potentials (−0.3 to −0.5 V), a small characteristic oxidation feature is observed, which is assigned to the oxidation of neutral Re^0−Re^0 dimeric species based on earlier reports involving $[Re(bpy)(CO)_3]_2$ complexes.[44,45] This peak is larger at fast scan rates and appears upon cycling through the second reduction. In comparison to the electrochemical behavior of **ReBpy**, we conclude that only a small fraction of $[Re^0(bpy)(CO)_3]^{\bullet}$ undergoes dimerization in the aniline-substituted complexes because of the added steric bulk of the ligand structure.

Cyclic voltammograms (CVs) under a wide range of scan rates show that the reductive peak currents ($i_{p,c}$) vary linearly versus the square root of the scan rate for all four complexes (Figures S16−S19), consistent with diffusion-controlled homogeneous systems. The diffusion coefficients (D) were determined by the Randles−Sevcik equation (eq 1) using the slopes of linear fits associated with the first reduction.[46]

$$i_p = 0.4463nFAC\left(\frac{nF\nu D}{RT}\right)^{1/2} \quad (1)$$

In this equation, i_p is the current response, F is Faraday's constant, A is the surface area of the electrode (0.07 cm^2 for the electrode used in this study), n is the number of electrons associated with the redox event, C is the concentration of the catalyst in solution, ν is the scan rate, R is the ideal gas constant, and T is the temperature in Kelvin.

Spectroelectrochemistry under N_2. IR-SEC has been a powerful tool for analyzing electrochemical reactions in real time and providing insight into the underlying mechanisms of rhenium and manganese tricarbonyl catalysts.[9] An optically transparent thin-layer electrochemical (OTTLE) cell[47] was used to monitor changes in the carbonyl stretching region of IR spectra of catalyst solutions under an applied potential. The experimental details are provided in the SI.

In their initial state, **1-Re**, **2-Re**, and **3-Re** show three carbonyl stretches (ν_{CO}) that are characteristic of *fac*-$Re(CO)_3$ complexes (Table 3). The C−O stretching frequencies of the aniline-substituted complexes are very similar to those of **ReBpy**.[48] Our IR-SEC experiments were limited to **1-Re** and **2-Re** due to the poor solubility of **3-Re** in CH_3CN. CVs of **1-Re** and **2-Re** in the OTTLE cell show two reduction waves similar to the CVs performed with a glassy carbon disk electrode. The C−O stretching frequencies observed for these compounds under reducing conditions are summarized in Table 4.

Table 3. Carbonyl Stretches of the Complexes under Study

catalyst	ν_{CO} (cm^{-1})	solvent
1-Re	2023, 1919, 1895	CH_3CN
2-Re	2022, 1919, 1892	CH_3CN
3-Re	2022, 1919, 1891	CH_3CN
ReBpy[48]	2021, 1914, 1897	CH_3CN

https://dx.doi.org/10.1021/acs.inorgchem.0c00154
Inorg. Chem. XXXX, XXX, XXX−XXX

Table 4. Experimental ν_{CO} Frequencies of Different Intermediates Detected by IR-SEC Experiments under N_2[a]

complex	**1-Re** (cm^{-1})	**2-Re** (cm^{-1})
$[Re(\mathbf{L})(CO)_3Cl]$	2023, 1919, 1895	2022, 1919, 1892
$[Re(\mathbf{L})(CO)_3Cl]^{\bullet-}$	2006, 1895, 1879	2000, 1889, 1863
$[Re(\mathbf{L})(CO)_3(CH_3CN)]^{\bullet}$		2007, 1892, 1871
$[Re(\mathbf{L})(CO)_3]^{\bullet}$	1984, 1865, 1853	1986, 1868, 1848
$[Re(\mathbf{L})(CO)_3]^{-}$	1947, 1847(br)	1946, 1848(br)
$[Re(\mathbf{L})(CO)_3(CH_3CN)]^{-}$		1992 (overlapped)

[a]The IR spectra are shown in Figure 5. Experimental ν_{CO} frequencies of related complexes are summarized in Table S2.

When the applied potential is held at the first reduction peak, the initial carbonyl signals start to diminish and a new set of lower-energy peaks begin to emerge. For **1-Re**, the ν_{CO} modes of the new species are red-shifted by ~20 cm^{-1} relative to the initial complex (Figure 5). This change in energy is consistent with a one-electron ligand-based reduction, and we assign this species to $[Re(\mathbf{L1})(CO)_3Cl]^{\bullet-}$, in accordance with previous studies.[18,48,49] Holding the potential at the tail of the first reduction peak forms the chloride-dissociated neutral species $[Re(\mathbf{L1})(CO)_3]^{\bullet}$, which results in another ~20−30 cm^{-1} red shift of the C−O vibrational modes. Scanning toward more negative potentials (onset of the second reduction wave) quickly gives rise to peaks corresponding to the five-coordinate $[Re(\mathbf{L1})(CO)_3]^{-}$ species at the expense of $[Re(\mathbf{L1})(CO)_3]^{\bullet}$. The two-electron-reduced intermediate $[Re(\mathbf{L1})(CO)_3]^{-}$ is widely proposed to be the catalytically active species that is responsible for CO_2 activation.[18,38,48] Although the C−O absorption bands of this species are overlapped by $[Re(\mathbf{L1})(CO)_3]^{\bullet}$ in the IR spectrum, the high-energy band of $[Re(\mathbf{L1})(CO)_3]^{-}$ at 1947 cm^{-1} (with a characteristic ~40 cm^{-1} shift relative to $[Re(\mathbf{L1})(CO)_3]^{\bullet}$) and a broad lower-energy band at 1847 cm^{-1} are clearly visible in the spectrum.[44,45]

IR-SEC of **2-Re** shows slightly different behavior relative to **1-Re**. At the first reduction potential, the C−O stretching frequencies shift to lower energies corresponding to $[Re(\mathbf{L2})(CO)_3Cl]^{\bullet-}$. However, this radical anion rapidly converts into a new species denoted by a shift in the carbonyl vibrational modes to higher energy, which is ascribed to the neutral CH_3CN-bound intermediate $[Re(bpy)(CO)_3(CH_3CN)]^{\bullet}$, consistent with previous IR-SEC studies.[23,48] This species is a result of rapid ligand exchange of the radical anion in a coordinating solvent (CH_3CN). Notably, this intermediate was not observed with **1-Re**, where labilization of the chloride ligand results in a five-coordinate neutral species. The steric bulk of the *ortho*-amine functionality presumably favors formation of the five-coordinate species over the six-coordinate solvent-bound complex. Likewise, increased electron density from the conjugated *o*-NH_2 group to the bipyridine donor could limit the formation of such an intermediate.

Interestingly, holding the potential just after the first reduction wave of **2-Re** concurrently forms the five-coordinate radical $[Re(\mathbf{L2})(CO)_3]^{\bullet}$ species and the two-electron-reduced $[Re(\mathbf{L2})(CO)_3]^{-}$ intermediate as a minor species. This behavior is rationalized by the expected close reduction potentials of pristine **2-Re** and the neutral species $[Re(\mathbf{L2})(CO)_3(MeCN)]^{\bullet}$ in light of similar observations of related rhenium complexes.[23,48] The peaks corresponding to the two-electron-reduced species grow in intensity when the potential is held for a longer time. A shoulder is also observed at 1992 cm^{-1} and tentatively assigned to the two-electron-reduced six-coordinate $[Re(\mathbf{L2})(CO)_3(CH_3CN)]^{-}$ species.[23,48,50] The lower-energy peak of this solvento species is likely obscured by the broad peak of $[Re(\mathbf{L2})(CO)_3]^{-}$.

The ν_{CO} frequencies of the proposed intermediates *en route* to generating the catalytically active species $[Re(\mathbf{L})(CO)_3]^{-}$ for both **1-Re** and **2-Re** and some related complexes are presented in Table S2. In **1-Re**, formation of the active species $[Re(\mathbf{L1})(CO)_3]^{-}$ was only observed at the second reduction potential. In contrast, the active species of **2-Re** was generated at the first reduction wave. CVs performed under catalytic conditions at a slower scan rate also support this observation (*vide infra*).

Notably, no dimeric intermediate was detected for any of our complexes during IR-SEC studies, presumably because of the steric demand of the aminophenyl substituents. However, in oxidative scans of CVs at fast scan rates, evidence of a dimeric species in small quantities was observed. This discrepancy prompted us to perform UV−vis spectroelectrochemistry (UV−vis SEC) to determine whether Re−Re bond formation was occurring under reducing conditions as the dimer has a characteristic absorption band centered around

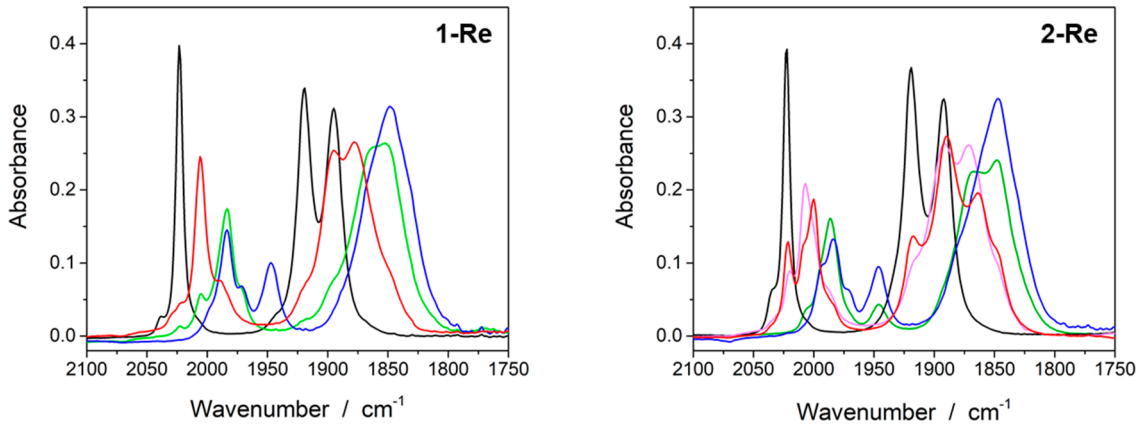

Figure 5. IR-SEC reduction of **1-Re** (left) and **2-Re** (right) under N_2. The assigned species are color-coded as follows: $Re(\mathbf{L})(CO)_3Cl$ (black), $[Re(\mathbf{L})(CO)_3Cl]^{\bullet-}$ (red), $[Re(\mathbf{L})(CO)_3(CH_3CN)]^{\bullet}$ (pink), $[Re(\mathbf{L})(CO)_3]^{\bullet}$ (green), $[Re(\mathbf{L})(CO)_3]^{-}$, and $[Re(\mathbf{L})(CO)_3(CH_3CN)]^{-}$ (blue), where L = bipyridyl ligand.

https://dx.doi.org/10.1021/acs.inorgchem.0c00154
Inorg. Chem. XXXX, XXX, XXX−XXX

800 nm.[36,44] Experimental details of the UV−vis SEC studies are given in the SI.

At an applied potential corresponding to the first reduction, a new absorption band at 521 nm appears in the UV−vis spectra of both **1-Re** and **2-Re** (Figure 6). This absorption is

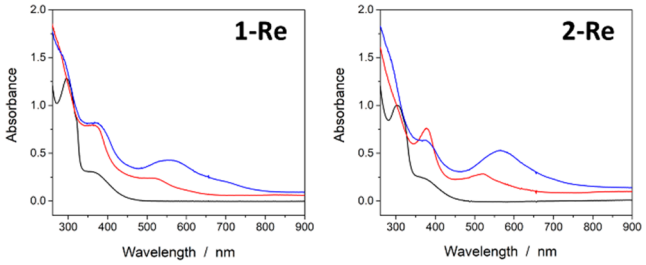

Figure 6. UV−vis SEC reduction of **1-Re** (left) and **2-Re** (right) under N_2. The assigned species are color-coded as follows: pristine complexes (black); one-electron-reduced species (red); two-electron-reduced species (blue).

assigned to the one-electron-reduced species, consistent with previous reports on related compounds.[36,42,51] Holding the potential at the second reduction gives rise to a new absorption feature with a λ_{max} value of 560 nm for **1-Re** and 566 nm for **2-Re**, which are comparable to previously reported two-electron-reduced rhenium bipyridyl complexes.[26,36,42] Notably, the characteristic absorption band for the Re−Re dimer is absent in the spectra of both complexes.

In previous studies, the Re^0−Re^0 dimer was also not observed during IR-SEC experiments with **ReBpy** in CH_3CN.[48] It was proposed that $[Re(bpy)(CO)_3]^\bullet$ reacts too quickly with the coordinating solvent for dimerization to occur.[39,48] It has also been shown spectroscopically that substitution with bulky *tert*-butyl groups at the 4 and 4′ positons of **ReBpy** slows down or prevents dimerization.[18,44] We reason that substitution at the 6 position of bipyridine will have a similar effect. Finally, the SEC and cyclic voltammetry experiments operate on different time scales.[23,48] This may be a contributing factor behind the absence of dimer in the SEC studies.

Electrochemical Studies under CO_2. Following the studies under an inert atmosphere, cyclic voltammetry was performed in CO_2-saturated anhydrous CH_3CN solutions to assess the catalytic activity of **1-Re**, **2-Re**, and **3-Re** for CO_2 reduction. The first redox event for all three complexes remains largely unchanged in the presence of substrate. Scanning toward more negative potentials gives rise to catalytic waves near the second reduction process (Figure 4). This behavior is comparable to that of **ReBpy**. From the IR-SEC results, **2-Re** is expected to form a small amount of reactive intermediate for CO_2 binding and reduction at the first reduction potential, which would allow catalysis to occur at a lower overpotential. Although this was not observed in CVs conducted at higher scan rates, the catalytic current does initiate at the first reduction of **2-Re** at slow scan rates (Figure S20). This behavior is not as prominent with the other complexes studied here, particularly **3-Re** and **ReBpy**. We note that similar results were obtained with ruthenium polypyridyl complexes by ligand modification, which altered the catalytic cycle and enabled catalysis at a lower overpotential.[52]

The overpotentials and catalytic current increases are considerably different for all four catalysts investigated in this work (Figure 4). Catalysts **1-Re**, **2-Re**, and **ReBpy** show crossing of the forward and return sweeps under CO_2 atmosphere, indicating that adsorption to the electrode surface or depletion of the substrate in the diffusion layer of the electrode may be taking place.[53,54] In general, the amino-phenyl-substituted catalysts exhibit higher catalytic currents relative to **ReBpy**. At a scan rate of 100 mV s^{-1}, **1-Re**, **2-Re**, **3-Re**, and **ReBpy** show 8.8-, 11.0-, 6.6-, and 4.4-fold current enhancements as measured by the ratio of the catalytic current (i_{cat}) relative to the reductive peak current observed in the absence of substrate (i_p). Complex **2-Re** shows the largest i_{cat}/i_p value from the series with a catalytic half-wave potential ($E_{cat/2}$) that is 50 mV more positive than that of **ReBpy** and 100 mV more positive than those of **1-Re** and **3-Re**. Importantly, this indicates that the catalytic activity in this series depends on factors other than mere catalytic overpotentials, since **3-Re** would be expected to be the most active catalyst of the series on the basis of thermodynamic driving force for CO_2 reduction.

The ratio of the catalytic current (i_{cat}) and corresponding reductive peak current in the absence of a substrate (i_p) serves as a useful gauge to compare the activity of different catalysts. According to the following electroanalytical equations (eqs 2 and 3), the catalytic rate constant (k_{cat}) and turnover frequency (TOF) are proportional to $(i_{cat}/i_p)^2$ under steady-state conditions (where n_p is 1, the number of electrons transferred in the noncatalytic reduction, and n_{cat} is 2 for CO_2 reduction to CO, the number of electrons transferred in the catalytic reaction).[54]

$$k_{obs} = k_{cat}[CO_2] \tag{2}$$

$$\text{TOF} = k_{obs} = \frac{Fvn_p^3}{RT}\left(\frac{0.4463}{n_{cat}}\right)^2\left(\frac{i_{cat}}{i_p}\right)^2 \tag{3}$$

Cyclic voltammetry as a function of the scan rate was performed in N_2- and CO_2-saturated solutions (Figure S21). From these data, i_{cat}/i_p values were obtained at each scan rate and TOFs were calculated using eq 3, which are plotted versus the scan rate in Figure S22. Although "S-shaped" catalytic waves were not observed with these systems, scan-rate-independent TOF values were obtained and are reported to allow a comparison to literature values. The estimated TOFs determined are 31.7, 98.8, 30.1, and 14.6 s^{-1} for **1-Re**, **2-Re**, **3-Re**, and **ReBpy**, respectively.

Deviations from ideal "S-shaped" catalytic waves in the CVs of these catalysts prompted us to apply foot-of-the-wave analysis (FOWA; eq 4). From this electroanalytical expression, k_{cat} can be determined and used to find the maximum TOF (TOF_{max}) under saturation conditions using eq 5.[55] In this method, the onset of the catalytic wave is analyzed in lieu of the peak catalytic current to avoid nonideal behavior, such as substrate depletion and catalyst deactivation, in calculating the rate of catalysis. The catalytic rate constant (k_{cat}) was determined from the linear portions of the slopes of plots of i/i_p versus $1/[1 + \exp\{(F/RT)(E - E_{cat})\}]$, where E_{cat} is the reduction potential of the catalyst associated with catalysis. The plots are shown in Figure S23, and the maximum TOFs obtained by FOWA are 45.5, 127, 58.8, and 21.2 s^{-1} for **1-Re**, **2-Re**, **3-Re**, and **ReBpy**, respectively. Table 5 contains $E_{cat/2}$, i_{cat}/i_p, and TOF values determined using both methods for all four catalysts. Noticeably, the TOF values determined by the two methods are comparable and display the same trend. In

https://dx.doi.org/10.1021/acs.inorgchem.0c00154
Inorg. Chem. XXXX, XXX, XXX−XXX

Table 5. Summary of the Results of Electrocatalysis in CO_2-Saturated Anhydrous CH_3CN[a]

catalyst	$E_{cat/2}$ (V)	i_{cat}/i_p	TOF (s^{-1})[b]	TOF (s^{-1})[c]
1-Re	−2.17	8.8	31.7	45.5
2-Re	−2.07	11.0	98.8	127
3-Re	−2.17	6.6	30.1	58.8
ReBpy	−2.12	4.4	14.6	21.2

[a]Potentials are referenced versus $Fc^{+/0}$ couple. The catalytic half-wave potential ($E_{cat/2}$), catalytic current (i_{cat}), and corresponding peak current in the absence of a substrate (i_p) were measured by cyclic voltammetry at ν = 100 mV s^{-1} in anhydrous CH_3CN/0.1 M Bu_4NPF_6. The reported TOF values have a standard deviation of <5%. [b]TOF calculated using eq 3. [c]TOF_{max} obtained from FOWA (eqs 4 and 5), where $E_{cat/2}$ was used for E_{cat} in eq 4.

general, the aminophenyl-substituted catalysts show faster rates than that of **ReBpy**, while **2-Re** is the most active system overall with a TOF that is 2.8, 2.2, and 6 times higher than the TOFs for **1-Re**, **3-Re**, and **ReBpy**, respectively.

$$\frac{i}{i_p} = \frac{2.24\sqrt{\frac{RT}{Fvn_p}}n_{cat}k_{cat}[CO_2]}{1 + \exp\left[\frac{F}{RT}(E - E_{cat})\right]} \quad (4)$$

$$TOF_{max} = k_{cat}[CO_2] \quad (5)$$

Effect of Brønsted Acids in CO_2 Reduction. Next, the catalytic activity of these systems was assessed in the presence of added external Brønsted acids in order to facilitate the proton-coupled reduction of CO_2. A wide range of proton sources have been used in the literature that have produced lower overpotentials (η) while enhancing the catalytic activity of various systems in organic solvents. However, it has also been observed, in the presence of proton sources, that the selectivity is compromised for some catalysts that favor H_2 evolution over CO_2 reduction due, in part, to the comparable standard potentials of these reactions.[7,56−58] We examined four weak Brønsted acids of different pK_a values in CH_3CN: water (H_2O; pK_a = 38−41),[59] methanol (pK_a = not reported), trifluoroethanol (TFE; pK_a = calcd 35.8),[60] and phenol (pK_a = 27.2).[61] In the presence of these acids, changes to the current response or peak shapes in the CVs of each catalyst under N_2-saturated conditions are minor, suggesting that the catalysts will have insignificant proton reduction activity in the potential window studied. Conversely, significant increases in the current are observed with the rhenium catalysts when CO_2 is introduced (Figure S24). The catalytic current begins at the onset of the first reduction in the presence of a proton source, which is markedly different from the anhydrous conditions (Figure 4).

Of the proton sources examined, TFE gives the highest i_{cat}/i_p value for the aniline-substituted catalysts and was chosen for the following experiments. A linear increase in the catalytic current as a function of the TFE concentration is observed initially with **1-Re** and **2-Re**, before reaching a maximum i_{cat}/i_p value at 4% TFE and subsequently dropping to lower values (Figure S30). This behavior is consistent with previous reports involving rhenium- and manganese-based electrocatalysts.[22,62,63]

The TOFs of each catalyst in CH_3CN/4% TFE solutions were estimated via cyclic voltammetry by applying the two electroanalytical methods described earlier (Figures S25−S27). The addition of an external proton source improved the rate of catalysis for each complex, as is evident by increases in the i_{cat}/i_p values and the calculated TOFs in the presence of 4% TFE, which are summarized in Table 6. The same trend in catalytic

Table 6. Summary of the Results of Electrocatalysis in CO_2-Saturated CH_3CN in the Presence of 4% TFE as the Proton Source[a]

catalyst	$E_{cat/2}$ (V)	i_{cat}/i_p	TOF (s^{-1})[b]	TOF (s^{-1})[c]
1-Re	−2.05	14.2	123	47.5
2-Re	−1.98	25.0	239	138
3-Re	−2.04	14.3	109	69.7
ReBpy	−1.98	13.4	72.9	47.5

[a]Potentials are referenced versus $Fc^{+/0}$ couple. The catalytic half-wave potentials ($E_{cat/2}$), catalytic currents (i_{cat}), and corresponding peak currents in the absence of a substrate (i_p) were measured by cyclic voltammetry at ν = 100 mV s^{-1} in CH_3CN/0.1 M Bu_4NPF_6 solutions containing 4% TFE. Reported TOF values have a standard deviation of <5%. [b]TOF calculated using eq 3. [c]TOF_{max} obtained from FOWA (eqs 4 and 5), where $E_{cat/2}$ was used for E_{cat} in eq 4.

activity is observed under protic conditions with **2-Re**, again, showing the best performance with a TOF of 239 s^{-1}. Catalysts **1-Re** and **3-Re** also exhibit better performances than the benchmark **ReBpy** system with TOFs of 123 and 109 s^{-1}, respectively.

The peak catalytic current (i_{cat}) for an electrocatalytic process that involves heterogeneous electron transfer can be expressed by the following electroanalytical equation:[64]

$$i_{cat} = n_{cat}FA[cat](Dk_{cat}[S]^y)^{1/2} \quad (6)$$

where [S] is the substrate concentration and [cat] is the catalyst concentration. This equation was used to investigate the reaction order with respect to the catalyst and substrate concentrations and to gain insight into the catalytic mechanism. Cyclic voltammetry was performed to record the current response (i_{cat}) under variable concentrations of CO_2, TFE, and catalyst by systematically changing the concentration of one species at a time. First, the catalyst concentration was varied from 0 to 0.5 mM in CO_2-saturated CH_3CN. A linear relationship is observed in plots of the peak catalytic current (i_{cat}) from each CV versus the concentration of catalyst, revealing a first-order dependence on the catalyst (Figure S28). The maximum catalyst concentration was restricted to 0.5 mM to avoid suspensions of the catalyst at higher concentrations in CH_3CN. Next, CVs were obtained where the CO_2 concentration was varied in CH_3CN solutions containing 0.5 mM catalyst. A first-order dependence on [CO_2] was determined (where y = 1) as the catalytic current increases linearly as a function of $\sqrt{[CO_2]^1}$ (Figure S29). The concentration of TFE was also varied from 0 to 4% (v/v) in CO_2-saturated CH_3CN with 0.5 mM catalyst and showed a linear increase in the plots of i_{cat} versus [TFE], indicating a second-order dependence on the acid ($\sqrt{[TFE]^2}$) (Figure S30). The rate law can be summarized as follows: rate = k[cat][CO_2][TFE]^2, which indicates that the second protonation event, resulting in C−O bond cleavage and the elimination of H_2O, is the rate-limiting step in this $2H^+/2e^-$ reduction of CO_2 to CO.[26,57]

Controlled Potential Electrolysis (CPE). Bulk electrolysis experiments were performed on the complexes using an airtight electrochemical cell with applied potentials corre-

https://dx.doi.org/10.1021/acs.inorgchem.0c00154
Inorg. Chem. XXXX, XXX, XXX−XXX

sponding to their peak catalytic currents in order to quantify products and to assess catalyst stability. The experiments were conducted with and without an external proton source to determine the efficiency, stability, and selectivity under both conditions. The experimental details are provided in the SI. The CPE results are summarized in Table 7 and shown graphically in Figure 7. Representative charge versus time plots are given in Figures S31 and S32.

Table 7. Summary of 1 h CPEs under Different Conditions[a]

catalyst	H^+ source	E_{appl} (V)[b]	charge (C)	FE_{CO} (%)
1-Re	4% TFE	−2.10	5.04 ± 0.10	89 ± 3
	none	−2.20	1.04 ± 0.03	38 ± 2
2-Re	4% TFE	−2.05	7.66 ± 0.23	93 ± 2
	none	−2.15	1.68 ± 0.07	83 ± 2
3-Re	4% TFE	−2.15	5.54 ± 0.08	98 ± 2
	none	−2.20	1.40 ± 0.04	52 ± 4
ReBpy	4% TFE	−2.12	3.65 ± 0.31	92 ± 3
	none	−2.15	1.17 ± 0.05	62 ± 2

[a]CPEs were performed with 0.5 mM catalyst concentration in CO_2-saturated CH_3CN/0.1 Bu_4NPF_6 solutions using a glassy carbon rod working electrode. Accumulated charges and FEs are reported as the average of three runs. [b]Applied potentials (vs $Fc^{+/0}$) correspond to the peak catalytic current observed for each system.

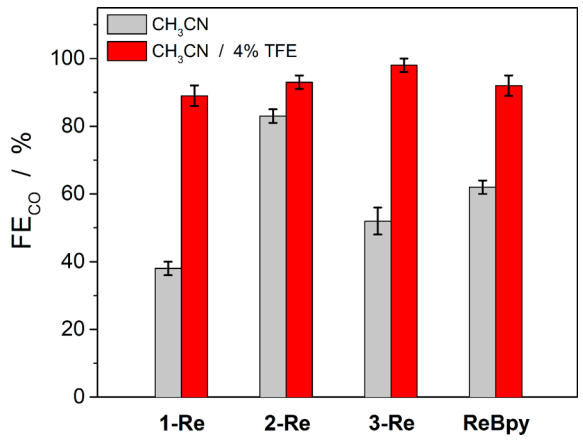

Figure 7. FEs from CPEs with 0.5 mM catalyst in CO_2-saturated CH_3CN/0.1 M Bu_4NPF_6 solutions under anhydrous conditions (gray) or with 4% TFE (red).

In these experiments, CO was found to be the sole carbon-containing product, and no H_2 was detected. These results demonstrate that all four catalysts strongly favor CO_2 reduction over H^+ reduction. In anhydrous solutions, **ReBpy** has a Faradaic efficiency (FE) of 62 ± 2%. This value is in agreement with previous reports.[56] Likewise, in the absence of TFE, **1-Re**, **2-Re**, and **3-Re** also show selective CO production with FEs of 38 ± 2%, 83 ± 2%, and 52 ± 4%, respectively. Interestingly, **2-Re** operates with a significantly higher FE compared to the other complexes in this study. The total amount of charge passed after 1 h for each system follows the same trend, with **2-Re** (1.68 ± 0.07 C) accumulating the most charge and **1-Re** passing the least amount of charge (1.04 ± 0.03 C). Notably, catalysis with **1-Re** slows down after ∼2 h, whereas **2-Re** and **3-Re** exhibit sustained catalysis for longer periods of time. This observation is consistent with the deactivation of **1-Re** during catalysis. In the absence of a proton source, the reductive disproportionation of CO_2 is often observed, where carbonate is formed as a coproduct of CO_2 reduction ($2CO_2 + 2e^- \rightarrow CO + CO_3^{2-}$). Here, 1 equiv of CO_2 is reduced to CO and the other CO_2 molecule acts as an "oxide acceptor" to generate CO_3^{2-}. Barium triflate was added to the filtered solutions following electrolyses, which caused significant precipitation of $BaCO_3$ for all three aniline-substituted catalysts, confirming the reductive disproportionation pathway under anhydrous conditions.[65−67] Moreover, analysis of the electrolyzed solution by FT-IR spectroscopy showed the emergence of strong bands at 1647 and 1683 cm^{-1}, which can be assigned to HCO_3^-/CO_3^{2-} species (Figure S33).[68,69]

A proton source was added to solutions to facilitate the proton-coupled reduction of CO_2, and large catalytic current enhancements were observed in the presence of TFE along with higher FEs for CO_2-to-CO conversion. Under these conditions, carbonate was not observed as a coproduct, consistent with the following reaction: $CO_2 + 2H^+ + 2e^- \rightarrow CO + H_2O$. The FEs for the four catalysts using TFE as a proton source are exceptional and range from 89 to 98% for CO production.

Rinse tests were performed after each CPE experiment to determine if any heterogeneous material had deposited onto the working electrode.[70] The post-CPE working electrodes did not show any sign of deposition, which suggests that the catalysts are homogeneous and do not adsorb to the electrode during bulk electrolysis experiments.

Structure and Activity. External Brønsted acids can have dramatic effects on the catalytic mechanism, especially when second-coordination-sphere functionality is present in the ligand framework. It was recently demonstrated in a manganese tricarbonyl catalyst with pendant ether groups and in macrocyclic cobalt catalysts with second-sphere amine groups that these groups can hydrogen-bond to the metal−carboxylic acid intermediate and/or orient a hydrogen-bonding network with Brønsted acid molecules to help stabilize the intermediate and accelerate C−O bond breaking and the elimination of H_2O.[63,71] The aniline-substituted complexes reported here are also expected to organize hydrogen-bonding interactions around the active site. Indeed, the crystal structure of **2-Re** shows the presence of a DMF solvent molecule that is hydrogen-bonded to the *meta*-amine group (Figure S34), which suggests that **2-Re** can orient Brønsted acid molecules toward the metal-bound substrate during catalysis, effectively increasing the local concentration of protons to enhance the activity.

In this work, the distance between the pendent amine and rhenium active site of each catalyst is well-defined and was systematically varied by preparing the *ortho*-, *meta*-, and *para*-substituted isomers to probe the structure−activity relationship. We anticipated that **1-Re** would have the highest activity within the series given the proximity of its amine to the active site, enabling direct and/or short-range hydrogen-bonding interactions during catalysis. Conversely, **3-Re** was expected to have modest improvements relative to **ReBpy** because its amine is oriented away from the metal center and limited to mediating long-range hydrogen-bonding networks or participating in intermolecular interactions. The expectation for **3-Re** was borne out by the data. Surprisingly, however, the activities of **1-Re** and **3-Re** are very similar and significantly lower than that of **2-Re**, which shows the fastest catalysis by a factor of 2 and at the lowest overpotential under both anhydrous and protic conditions.

https://dx.doi.org/10.1021/acs.inorgchem.0c00154
Inorg. Chem. XXXX, XXX, XXX−XXX

The shortest distance between the amine functionality and metal center is found in **1-Re**. Under anhydrous conditions, **1-Re** performs poorly during CPE experiments relative to its isomeric counterparts, and catalysis slows down after ∼4 turnovers. This behavior indicates probable deactivation of **1-Re** during catalysis in the absence of a proton source. In fact, κ^3 chelation of ligand **L1** with first- and second-row transition metals is known in the literature, where **L1** acts as an *N*,*N*′,*N*″-tridentate ligand and coordinates in a distorted meridional fashion.[72] During the catalytic cycle (following chloride dissociation from the precatalyst), **1-Re** likely forms a deactivated species in which the $-NH_2$ nitrogen atom binds to the open coordination site needed for substrate activation and catalysis, which may explain the lower than expected activity of this system. A related compound $[Re(bpy)(CO)_3(NH_2Ph)]^+$ bearing an aniline ligand has also been reported in the literature.[73] In addition, $Mn(\kappa^2\text{-}N,N'\text{-terpyridine})(CO)_3Br$ was recently investigated as an electrocatalyst for CO_2 reduction, where the bidentate terpyridine shifts to a κ^3-*N*,*N*′,*N*″ coordination mode during catalysis, ultimately leading to catalyst deactivation.[74] Several attempts to synthesize the proposed deactivated species of **1-Re** were unsuccessful in our laboratory. We note that, in the presence of TFE, catalysis with **1-Re** is sustained for a longer period of time and was comparable to that the other catalysts within the series.

On the basis of the results of IR-SEC experiments, we hypothesize that **2-Re** forms the catalytically active species at a lower potential than its aniline-substituted counterparts, giving **2-Re** a unique advantage during catalysis. This electronic effect, along with the position of its hydrogen-bond-donating amine group in the second coordination sphere, which is close enough to enhance catalysis while avoiding deactivation, makes **2-Re** the best catalyst of the series and a significantly more active catalyst relative to **ReBpy**.

Comparison to Related Catalysts. Despite being known in the literature for more than 3 decades, installing second-coordination-sphere functionalities in *fac*-$Re(bpy)(CO)_3$-type catalysts is a relatively new avenue of research. Previously, researchers appended phenolic groups, secondary and tertiary amines, thiourea moieties, and positively charged imidazolium groups to **ReBpy**-based catalysts, which aimed to stabilize the metal carboxylate and/or metal−carboxylic acid intermediates or to promote proton-transfer events that lead to C−O bond cleavage (Figure 8 and Table 8).[8,9,75]

Inspired by the high activity of **ReBpy** in room temperature ionic liquid,[76] Nippe and co-workers have incorporated imidazolium functionalities into the bipyridine framework to assess the *intramolecular* effect of these cationic substituents on catalysis (**1**).[22] Similar i_{cat}/i_p values relative to **ReBpy** were observed but at a ∼170 mV more positive potential. The decrease in overpotential was attributed to an intramolecular hydrogen-bonding interaction between the imidazolium C2−H hydrogen atom and Cl^- ligand, which was proposed to accelerate Cl^- dissociation following the first reduction. A higher i_{cat}/i_p value is observed in the presence of an added Brønsted acid.[22]

Marinescu and co-workers recently reported a series of rhenium complexes featuring pendant secondary and tertiary amines at the 6 and 6′ positions of 2,2′-bipyridine.[24] In contrast to our system, the reported complexes have the amines directly attached to the bipyridine ligand. Overall, the monosubstituted complexes (**2a** and **2b**) outperform their disubstituted counterparts in terms of stability, TON, and FE. No TOF values were reported in the study, but the i_{cat}/i_p values in anhydrous CH_3CN and in the presence of TFE clearly indicate that catalyst **2b** mediates the fastest catalysis within the series. However, the E_{cat} values are more negative than that of **ReBpy** due to the added electron density from the amine groups. The addition of a Brønsted acid improves the catalytic current response and allows moderate FEs ranging from 51 to 73% for the reported complexes.[24]

Neumann and co-workers have reported a **ReBpy** derivative that has a thiourea moiety tethered in the second coordination sphere (**3**).[21] The thiourea tether features an electron-withdrawing $-PhCF_3$ group, which increases the acidity of the hydrogen atoms and enhances the probable interaction with CO_2 molecules. Interestingly, thiourea in this catalyst acts as a local proton source during the catalytic cycle, and the addition of an external proton source inhibits catalysis.[21] This is in contrast to our system and other reported catalysts utilizing amine or amide functional groups in the second coordination sphere because these groups tend to form hydrogen bonds with the catalytic intermediates or neighboring Brønsted acid molecules instead of donating protons.[71,77]

Nervi and co-workers reported two rhenium tricarbonyl catalysts containing 1,3-dihydroxyphenyl (pdbpy) and 3,4,5-

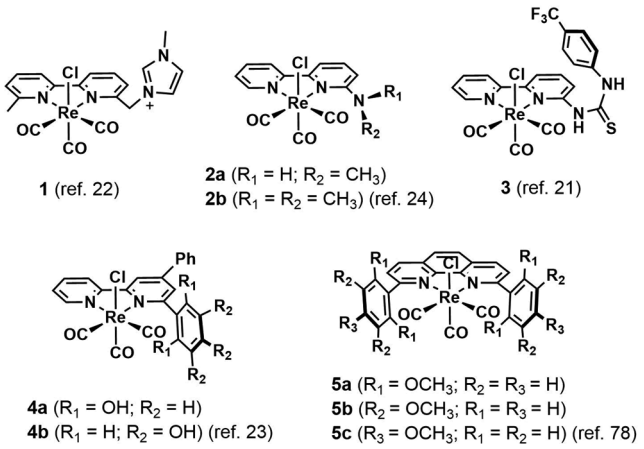

Figure 8. Related rhenium catalysts for CO_2 reduction with pendant functionality in the second coordination sphere.

Table 8. Catalytic Performance of Previously Reported Rhenium Complexes Containing Second-Coordination-Sphere Functionality[a]

catalyst	conditions	$E_{cat/2}$ (V)	FE_{CO} (%)	i_{cat}/i_p	TOF (s^{-1})	ref
1	dry CH_3CN	−1.87	NR	4.7	NR	22
	2−3 M H_2O/CH_3CN	NR	70[b]	12	∼270	22
2a	2 M TFE/CH_3CN	−2.06[c]	73	18.3	NR	24
2b	2 M TFE/CH_3CN	−2.32[c]	58	29.5	NR	24
3	dry CH_3CN	NR	89	NR	3040[d]	21
4a	5% H_2O/CH_3CN	NR	88	NR	NR	23
4b	5% H_2O/CH_3CN	NR	70	NR	NR	23
5a	dry DMF	−2.59	84	10.3	NR	78
5b	dry DMF	−2.32	17	4.7	NR	78
5c	dry DMF	−2.37	40	5	NR	78

[a]Catalyst structures are presented in Figure 8. NR = not reported. [b]CPE was done in 9.4 M H_2O/CH_3CN. [c]E_{cat}. [d]TOF_{max} value was reported.[21]

https://dx.doi.org/10.1021/acs.inorgchem.0c00154
Inorg. Chem. XXXX, XXX, XXX−XXX

trihydroxyphenyl (ptbpy) groups attached to the 6 position of a 4-phenyl-2,2′-bipyridine framework.[23] Although TOF or k_{cat} values were not reported, apparent i_{cat}/i_p values of ∼2.2 and ∼1.5 were obtained for **4a** and **4b**, respectively, in anhydrous CH_3CN. IR-SEC experiments under argon with **4a** reveal the reductive deprotonation of one of the hydroxyl substituents after the first reduction and subsequent formation of a Re−O bond. Upon reduction of this intermediate, a doubly deprotonated anionic intermediate is formed. IR-SEC under CO_2-saturated conditions shows that the deprotonated intermediate with a Re−O bond is the active catalytic species. The catalysts also have significantly different FEs in the absence or presence of external Brønsted acids. In anhydrous solutions, **4a** has a FE for CO production of 49%, whereas the FE for **4b** is 70%.[23] This is similar to our findings, where *meta*-substituted **2-Re** performed better than *ortho*-substituted **1-Re** in anhydrous solutions.

White and co-workers recently reported a series of rhenium complexes with methoxy-substituted 2,9-diphenyl-1,10-phenanthroline ligands where methoxy groups are systematically positioned around the phenyl groups in the *ortho*, *meta*, and *para* positions (**5a**, **5b**, and **5c**).[78] In contrast to our results, an *o*-methoxy-substituted rhenium complex showed the best catalytic performance, which was attributed to the formation of a more nucleophilic rhenium center that can activate CO_2 more effectively relative to the other isomers but at the expense of a higher overpotential.[78]

CONCLUSION

The synthesis, characterization, and electrocatalytic CO_2 reduction activity of a novel series of *fac*-$Re(CO)_3$ complexes have been reported here and compared to the unsubstituted benchmark **ReBpy** catalyst. The bipyridyl ligand was decorated with aniline-based hydrogen-bond donors, and the distance between the $-NH_2$ group and the catalytic center of each complex was varied systematically across the series. Catalysts **1-Re**, **2-Re**, and **3-Re** are highly selective for CO_2 reduction with FEs of ≥89% for CO evolution in the presence of a proton source. Notably, the TOF of **2-Re** is significantly better, no less than twice as high, compared to the rest of the catalysts investigated here in both anhydrous and protic conditions. IR-SEC and cyclic voltammetry experiments suggest that **2-Re** can access the catalytically active two-electron-reduced species at lower overpotentials. Moreover, **1-Re** suffers from deactivation, as indicated by its low stability during bulk electrolysis experiments. We reason that the relatively short distance between the $-NH_2$ group of **1-Re** and the rhenium active site results in coordination of the amine to the reduced metal center during catalysis and subsequent deactivation of the catalyst. The position of the second-coordination-sphere functionality relative to the active site must be carefully considered in order to enhance the catalytic activity while avoiding catalyst deactivation and/or unintended electronic effects. Ongoing efforts in our laboratory include the methylation of these aniline groups to access quaternary ammonium groups to investigate the influence of through-space charge interactions on catalysis.

ASSOCIATED CONTENT

Supporting Information

The Supporting Information is available free of charge at https://pubs.acs.org/doi/10.1021/acs.inorgchem.0c00154.

Experimental details, synthetic procedures, characterization of the rhenium compounds, crystal data and refinement details, and electrochemical and SEC results (PDF)

Accession Codes

CCDC 1976889 and 1976890 contain the supplementary crystallographic data for this paper. These data can be obtained free of charge via www.ccdc.cam.ac.uk/data_request/cif, or by emailing data_request@ccdc.cam.ac.uk, or by contacting The Cambridge Crystallographic Data Centre, 12 Union Road, Cambridge CB2 1EZ, UK; fax: +44 1223 336033.

AUTHOR INFORMATION

Corresponding Author

Jonah W. Jurss − *Department of Chemistry and Biochemistry, University of Mississippi, University, Mississippi 38677, United States;* orcid.org/0000-0002-2780-3415; Email: jwjurss@olemiss.edu

Authors

Kallol Talukdar − *Department of Chemistry and Biochemistry, University of Mississippi, University, Mississippi 38677, United States;* orcid.org/0000-0001-5480-9276

Sayontani Sinha Roy − *Department of Chemistry and Biochemistry, University of Mississippi, University, Mississippi 38677, United States;* orcid.org/0000-0002-2663-2810

Eva Amatya − *Department of Chemistry and Biochemistry, University of Mississippi, University, Mississippi 38677, United States*

Elizabeth A. Sleeper − *Department of Chemistry and Biochemistry, University of Mississippi, University, Mississippi 38677, United States*

Pierre Le Magueres − *Rigaku Americas Corporation, The Woodlands, Texas 77381, United States*

Complete contact information is available at: https://pubs.acs.org/10.1021/acs.inorgchem.0c00154

Author Contributions

†K.T. and S.S.R. contributed equally.

Notes

The authors declare no competing financial interest.

ACKNOWLEDGMENTS

We thank the National Science Foundation for generous support through seed grant funding OIA-1539035 and a CAREER Award CHE-1848478.

REFERENCES

(1) Solomon, S.; Plattner, G.-K.; Knutti, R.; Friedlingstein, P. Irreversible Climate Change Due to Carbon Dioxide Emissions. *Proc. Natl. Acad. Sci. U. S. A.* **2009**, *106* (6), 1704−1709.

(2) Sarmiento, J. L.; Hughes, T. M. C.; Stouffer, R. J.; Manabe, S. Simulated Response of the Ocean Carbon Cycle to Anthropogenic Climate Warming. *Nature* **1998**, *393* (6682), 245−249.

(3) Davis, S. J.; Caldeira, K.; Matthews, H. D. Future CO2 Emissions and Climate Change from Existing Energy Infrastructure. *Science* **2010**, *329* (5997), 1330−1333.

(4) Lüthi, D.; Le Floch, M. L.; Bereiter, B.; Blunier, T.; Barnola, J.-M.; Siegenthaler, U.; Raynaud, D.; Jouzel, J.; Fischer, H.; Kawamura, K.; Stocker, T. F. High-Resolution Carbon Dioxide Concentration Record 650,000−800,000 Years before Present. *Nature* **2008**, *453* (7193), 379−382.

(5) Finn, C.; Schnittger, S.; Yellowlees, L. J.; Love, J. B. Molecular Approaches to the Electrochemical Reduction of Carbon Dioxide. *Chem. Commun.* **2012**, *48* (10), 1392−1399.
(6) DuBois, D. L. Development of Molecular Electrocatalysts for Energy Storage. *Inorg. Chem.* **2014**, *53* (8), 3935−3960.
(7) Elgrishi, N.; Chambers, M. B.; Wang, X.; Fontecave, M. Molecular Polypyridine-Based Metal Complexes as Catalysts for the Reduction of CO2. *Chem. Soc. Rev.* **2017**, *46* (3), 761−796.
(8) Appel, A. M.; Bercaw, J. E.; Bocarsly, A. B.; Dobbek, H.; DuBois, D. L.; Dupuis, M.; Ferry, J. G.; Fujita, E.; Hille, R.; Kenis, P. J. A.; Kerfeld, C. A.; Morris, R. H.; Peden, C. H. F.; Portis, A. R.; Ragsdale, S. W.; Rauchfuss, T. B.; Reek, J. N. H.; Seefeldt, L. C.; Thauer, R. K.; Waldrop, G. L. Frontiers, Opportunities, and Challenges in Biochemical and Chemical Catalysis of CO2 Fixation. *Chem. Rev.* **2013**, *113* (8), 6621−6658.
(9) Francke, R.; Schille, B.; Roemelt, M. Homogeneously Catalyzed Electroreduction of Carbon Dioxide—Methods, Mechanisms, and Catalysts. *Chem. Rev.* **2018**, *118* (9), 4631−4701.
(10) Jeoung, J.-H.; Dobbek, H. Carbon Dioxide Activation at the Ni, Fe-Cluster of Anaerobic Carbon Monoxide Dehydrogenase. *Science* **2007**, *318* (5855), 1461−1464.
(11) Boyington, J. C.; Gladyshev, V. N.; Khangulov, S. V.; Stadtman, T. C.; Sun, P. D. Crystal Structure of Formate Dehydrogenase H: Catalysis Involving Mo, Molybdopterin, Selenocysteine, and an Fe4S4 Cluster. *Science* **1997**, *275* (5304), 1305−1308.
(12) Nichols, A. W.; Machan, C. W. Secondary-Sphere Effects in Molecular Electrocatalytic CO_2 Reduction. *Front. Chem.* **2019**, *7*. DOI: 10.3389/fchem.2019.00397.
(13) Shook, R. L.; Borovik, A. S. Role of the Secondary Coordination Sphere in Metal-Mediated Dioxygen Activation. *Inorg. Chem.* **2010**, *49* (8), 3646−3660.
(14) Margarit, C. G.; Schnedermann, C.; Asimow, N. G.; Nocera, D. G. Carbon Dioxide Reduction by Iron Hangman Porphyrins. *Organometallics* **2019**, *38* (6), 1219−1223.
(15) Margarit, C. G.; Asimow, N. G.; Gonzalez, M. I.; Nocera, D. G. Double Hangman Iron Porphyrin and the Effect of Electrostatic Nonbonding Interactions on Carbon Dioxide Reduction. *J. Phys. Chem. Lett.* **2020**, *11* (5), 1890−1895.
(16) Costentin, C.; Drouet, S.; Robert, M.; Savéant, J.-M. A Local Proton Source Enhances CO2 Electroreduction to CO by a Molecular Fe Catalyst. *Science* **2012**, *338* (6103), 90−94.
(17) Azcarate, I.; Costentin, C.; Robert, M.; Savéant, J.-M. Through-Space Charge Interaction Substituent Effects in Molecular Catalysis Leading to the Design of the Most Efficient Catalyst of CO2-to-CO Electrochemical Conversion. *J. Am. Chem. Soc.* **2016**, *138* (51), 16639−16644.
(18) Smieja, J. M.; Kubiak, C. P. Re(Bipy-TBu)(CO)3Cl-improved Catalytic Activity for Reduction of Carbon Dioxide: IR-Spectroelectrochemical and Mechanistic Studies. *Inorg. Chem.* **2010**, *49* (20), 9283−9289.
(19) Wong, K.-Y.; Chung, W.-H.; Lau, C.-P. The Effect of Weak Brönsted Acids on the Electrocatalytic Reduction of Carbon Dioxide by a Rhenium Tricarbonyl Bipyridyl Complex. *J. Electroanal. Chem.* **1998**, *453* (1), 161−170.
(20) Grice, K. A.; Kubiak, C. P. Recent Studies of Rhenium and Manganese Bipyridine Carbonyl Catalysts for the Electrochemical Reduction of CO_2. In *Advances in Inorganic Chemistry*; Aresta, M., van Eldik, R., Eds.; Academic Press, 2014; Vol. *66*, Chapter 5, pp 163−188; DOI: 10.1016/B978-0-12-420221-4.00005-6.
(21) Haviv, E.; Azaiza-Dabbah, D.; Carmieli, R.; Avram, L.; Martin, J. M. L.; Neumann, R. A Thiourea Tether in the Second Coordination Sphere as a Binding Site for CO2 and a Proton Donor Promotes the Electrochemical Reduction of CO2 to CO Catalyzed by a Rhenium Bipyridine-Type Complex. *J. Am. Chem. Soc.* **2018**, *140* (39), 12451−12456.
(22) Sung, S.; Kumar, D.; Gil-Sepulcre, M.; Nippe, M. Electrocatalytic CO2 Reduction by Imidazolium-Functionalized Molecular Catalysts. *J. Am. Chem. Soc.* **2017**, *139* (40), 13993−13996.
(23) Rotundo, L.; Garino, C.; Priola, E.; Sassone, D.; Rao, H.; Ma, B.; Robert, M.; Fiedler, J.; Gobetto, R.; Nervi, C. Electrochemical and Photochemical Reduction of CO2 Catalyzed by Re(I) Complexes Carrying Local Proton Sources. *Organometallics* **2019**, *38* (6), 1351−1360.
(24) Hellman, A. N.; Haiges, R.; Marinescu, S. C. Rhenium Bipyridine Catalysts with Hydrogen Bonding Pendant Amines for CO2 Reduction. *Dalton Trans.* **2019**, *48* (38), 14251−14255.
(25) Chabolla, S. A.; Machan, C. W.; Yin, J.; Dellamary, E. A.; Sahu, S.; Gianneschi, N. C.; Gilson, M. K.; Tezcan, F. A.; Kubiak, C. P. Bio-Inspired CO2 Reduction by a Rhenium Tricarbonyl Bipyridine-Based Catalyst Appended to Amino Acids and Peptidic Platforms: Incorporating Proton Relays and Hydrogen-Bonding Functional Groups. *Faraday Discuss.* **2017**, *198* (0), 279−300.
(26) Yang, W.; Sinha Roy, S.; Pitts, W. C.; Nelson, R. L.; Fronczek, F. R.; Jurss, J. W. Electrocatalytic CO2 Reduction with Cis and Trans Conformers of a Rigid Dinuclear Rhenium Complex: Comparing the Monometallic and Cooperative Bimetallic Pathways. *Inorg. Chem.* **2018**, *57* (15), 9564−9575.
(27) Liyanage, N. P.; Yang, W.; Guertin, S.; Sinha Roy, S.; Carpenter, C. A.; Adams, R. E.; Schmehl, R. H.; Delcamp, J. H.; Jurss, J. W. Photochemical CO2 Reduction with Mononuclear and Dinuclear Rhenium Catalysts Bearing a Pendant Anthracene Chromophore. *Chem. Commun.* **2019**, *55* (7), 993−996.
(28) Wilting, A.; Stolper, T.; Mata, R. A.; Siewert, I. Dinuclear Rhenium Complex with a Proton Responsive Ligand as a Redox Catalyst for the Electrochemical CO2 Reduction. *Inorg. Chem.* **2017**, *56* (7), 4176−4185.
(29) Miyaura, N.; Suzuki, A. Palladium-Catalyzed Cross-Coupling Reactions of Organoboron Compounds. *Chem. Rev.* **1995**, *95* (7), 2457−2483.
(30) Caspar, J. V.; Meyer, T. J. Application of the Energy Gap Law to Nonradiative, Excited-State Decay. *J. Phys. Chem.* **1983**, *87* (6), 952−957.
(31) Lense, S.; Guzei, I. A.; Andersen, J.; Thao, K. C. Crystal Structures of a Manganese(I) and a Rhenium(I) Complex of a Bipyridine Ligand with a Non-Coordinating Benzoic Acid Moiety. *Acta Crystallogr. Sect. E Crystallogr. Commun.* **2018**, *74* (5), 731−736.
(32) Xia, H.; Liu, X.; Wu, Q.; Zhang, Y.; Gao, W.; Mu, Y. Synthesis, Structure, and Luminescence of Rhenium(I) Complexes with Substituted Bipyridines. *J. Coord. Chem.* **2012**, *65* (7), 1266−1277.
(33) Martinez, J. F.; La Porte, N. T.; Chaudhuri, S.; Sinopoli, A.; Bae, Y. J.; Sohail, M.; Batista, V. S.; Wasielewski, M. R. Effect of Electronic Coupling on Electron Transfer Rates from Photoexcited Naphthalenediimide Radical Anion to Re(Bpy)(CO)3X. *J. Phys. Chem. C* **2019**, *123* (16), 10178−10190.
(34) Kurz, P.; Probst, B.; Spingler, B.; Alberto, R. Ligand Variations in [ReX(Diimine)(CO)3] Complexes: Effects on Photocatalytic CO2 Reduction. *Eur. J. Inorg. Chem.* **2006**, *2006* (15), 2966−2974.
(35) Sullivan, B. P.; Bolinger, C. M.; Conrad, D.; Vining, W. J.; Meyer, T. J. One- and Two-Electron Pathways in the Electrocatalytic Reduction of CO2 by Fac-Re(Bpy)(CO)3Cl (Bpy = 2,2′-Bipyridine). *J. Chem. Soc., Chem. Commun.* **1985**, No. 20, 1414−1416.
(36) Fujita, E.; Muckerman, J. T. Why Is Re-Re Bond Formation/Cleavage in [Re(Bpy)(CO)3]2 Different from That in [Re(CO)5]2? Experimental and Theoretical Studies on the Dimers and Fragments. *Inorg. Chem.* **2004**, *43* (24), 7636−7647.
(37) Benson, E. E.; Sampson, M. D.; Grice, K. A.; Smieja, J. M.; Froehlich, J. D.; Friebel, D.; Keith, J. A.; Carter, E. A.; Nilsson, A.; Kubiak, C. P. The Electronic States of Rhenium Bipyridyl Electrocatalysts for CO2 Reduction as Revealed by X-Ray Absorption Spectroscopy and Computational Quantum Chemistry. *Angew. Chem., Int. Ed.* **2013**, *52* (18), 4841−4844.
(38) Sampson, M. D.; Froehlich, J. D.; Smieja, J. M.; Benson, E. E.; Sharp, I. D.; Kubiak, C. P. Direct Observation of the Reduction of Carbon Dioxide by Rhenium Bipyridine Catalysts. *Energy Environ. Sci.* **2013**, *6* (12), 3748−3755.
(39) O'Toole, T. R.; Younathan, J. N.; Sullivan, B. P.; Meyer, T. J. 1,2-Difluorobenzene: A Relatively Inert and Noncoordinating Solvent

https://dx.doi.org/10.1021/acs.inorgchem.0c00154
Inorg. Chem. XXXX, XXX, XXX−XXX

for Electrochemical Studies on Transition-Metal Complexes. *Inorg. Chem.* **1989**, *28* (20), 3923−3926.
(40) Stanton, C. J.; Machan, C. W.; Vandezande, J. E.; Jin, T.; Majetich, G. F.; Schaefer, H. F.; Kubiak, C. P.; Li, G.; Agarwal, J. Re(I) NHC Complexes for Electrocatalytic Conversion of CO2. *Inorg. Chem.* **2016**, *55* (6), 3136−3144.
(41) Paolucci, F.; Marcaccio, M.; Paradisi, C.; Roffia, S.; Bignozzi, C. A.; Amatore, C. Dynamics of the Electrochemical Behavior of Diimine Tricarbonyl Rhenium(I) Complexes in Strictly Aprotic Media. *J. Phys. Chem. B* **1998**, *102* (24), 4759−4769.
(42) Breikss, A. I.; Abruña, H. D. Electrochemical and Mechanistic Studies of Re(CO)3(Dmbpy)CI] and Their Relation to the Catalytic Reduction of CO2. *J. Electroanal. Chem. Interfacial Electrochem.* **1986**, *201* (2), 347−358.
(43) Manbeck, G. F.; Muckerman, J. T.; Szalda, D. J.; Himeda, Y.; Fujita, E. Push or Pull? Proton Responsive Ligand Effects in Rhenium Tricarbonyl CO2 Reduction Catalysts. *J. Phys. Chem. B* **2015**, *119* (24), 7457−7466.
(44) Hayashi, Y.; Kita, S.; Brunschwig, B. S.; Fujita, E. Involvement of a Binuclear Species with the Re-C(O)O-Re Moiety in CO2 Reduction Catalyzed by Tricarbonyl Rhenium(I) Complexes with Diimine Ligands: Strikingly Slow Formation of the Re-Re and Re-C(O)O-Re Species from Re(Dmb)(CO)3S (Dmb = 4,4′-Dimethyl-2,2′-Bipyridine, S = Solvent). *J. Am. Chem. Soc.* **2003**, *125* (39), 11976−11987.
(45) Benson, E. E.; Kubiak, C. P. Structural Investigations into the Deactivation Pathway of the CO2 Reduction Electrocatalyst Re(Bpy)(CO)3Cl. *Chem. Commun.* **2012**, *48* (59), 7374−7376.
(46) Bard, A. J.; Faulkner, L. R. *Electrochemical Methods: Fundamentals and Applications*, 2nd ed.; John Wiley and Sons: New York, 2000.
(47) Krejčik, M.; Daněk, M.; Hartl, F. Simple Construction of an Infrared Optically Transparent Thin-Layer Electrochemical Cell: Applications to the Redox Reactions of Ferrocene, Mn2(CO)10 and Mn(CO)3(3,5-Di-t-Butyl-Catecholate)-. *J. Electroanal. Chem. Interfacial Electrochem.* **1991**, *317* (1), 179−187.
(48) Johnson, F. P. A.; George, M. W.; Hartl, F.; Turner, J. J. Electrocatalytic Reduction of CO2 Using the Complexes [Re(Bpy)(CO)3L]n (n = + 1, L = P(OEt)3, CH3CN; n = 0, L = Cl-, Otf-; Bpy = 2,2′-Bipyridine; Otf- = CF3SO3) as Catalyst Precursors: Infrared Spectroelectrochemical Investigation. *Organometallics* **1996**, *15* (15), 3374−3387.
(49) Stor, G. J.; Hartl, F.; van Outersterp, J. W. M.; Stufkens, D. J. Spectroelectrochemical (IR, UV/Vis) Determination of the Reduction Pathways for a Series of [Re(CO)3(.Alpha.-Diimine)L']0/+ (L' = Halide, OTf-, THF, MeCN, n-PrCN, PPh3, P(OMe)3) Complexes. *Organometallics* **1995**, *14* (3), 1115−1131.
(50) Machan, C. W.; Chabolla, S. A.; Kubiak, C. P. Reductive Disproportionation of Carbon Dioxide by an Alkyl-Functionalized Pyridine Monoimine Re(I) Fac-Tricarbonyl Electrocatalyst. *Organometallics* **2015**, *34* (19), 4678−4683.
(51) Takeda, H.; Koike, K.; Inoue, H.; Ishitani, O. Development of an Efficient Photocatalytic System for CO2 Reduction Using Rhenium(I) Complexes Based on Mechanistic Studies. *J. Am. Chem. Soc.* **2008**, *130* (6), 2023−2031.
(52) Johnson, B. A.; Maji, S.; Agarwala, H.; White, T. A.; Mijangos, E.; Ott, S. Activating a Low Overpotential CO2 Reduction Mechanism by a Strategic Ligand Modification on a Ruthenium Polypyridyl Catalyst. *Angew. Chem., Int. Ed.* **2016**, *55* (5), 1825−1829.
(53) Martin, D. J.; McCarthy, B. D.; Rountree, E. S.; Dempsey, J. L. Qualitative Extension of the EC′ Zone Diagram to a Molecular Catalyst for a Multi-Electron, Multi-Substrate Electrochemical Reaction. *Dalton Trans.* **2016**, *45* (24), 9970−9976.
(54) Rountree, E. S.; McCarthy, B. D.; Eisenhart, T. T.; Dempsey, J. L. Evaluation of Homogeneous Electrocatalysts by Cyclic Voltammetry. *Inorg. Chem.* **2014**, *53* (19), 9983−10002.
(55) Costentin, C.; Drouet, S.; Robert, M.; Savéant, J.-M. Turnover Numbers, Turnover Frequencies, and Overpotential in Molecular Catalysis of Electrochemical Reactions. Cyclic Voltammetry and Preparative-Scale Electrolysis. *J. Am. Chem. Soc.* **2012**, *134* (27), 11235−11242.
(56) Liyanage, N. P.; Dulaney, H. A.; Huckaba, A. J.; Jurss, J. W.; Delcamp, J. H. Electrocatalytic Reduction of CO2 to CO With Re-Pyridyl-NHCs: Proton Source Influence on Rates and Product Selectivities. *Inorg. Chem.* **2016**, *55* (12), 6085−6094.
(57) Su, X.; McCardle, K. M.; Chen, L.; Panetier, J. A.; Jurss, J. W. Robust and Selective Cobalt Catalysts Bearing Redox-Active Bipyridyl-N-Heterocyclic Carbene Frameworks for Electrochemical CO2 Reduction in Aqueous Solutions. *ACS Catal.* **2019**, *9* (8), 7398−7408.
(58) Su, X.; McCardle, K. M.; Panetier, J. A.; Jurss, J. W. Electrocatalytic CO2 Reduction with Nickel Complexes Supported by Tunable Bipyridyl-N-Heterocyclic Carbene Donors: Understanding Redox-Active Macrocycles. *Chem. Commun.* **2018**, *54* (27), 3351−3354.
(59) McCarthy, B. D.; Martin, D. J.; Rountree, E. S.; Ullman, A. C.; Dempsey, J. L. Electrochemical Reduction of Brønsted Acids by Glassy Carbon in Acetonitrile—Implications for Electrocatalytic Hydrogen Evolution. *Inorg. Chem.* **2014**, *53* (16), 8350−8361.
(60) Lam, Y. C.; Nielsen, R. J.; Gray, H. B.; Goddard, W. A. A Mn Bipyrimidine Catalyst Predicted To Reduce CO2 at Lower Overpotential. *ACS Catal.* **2015**, *5* (4), 2521−2528.
(61) Felton, G. A. N.; Glass, R. S.; Lichtenberger, D. L.; Evans, D. H. Iron-Only Hydrogenase Mimics. Thermodynamic Aspects of the Use of Electrochemistry to Evaluate Catalytic Efficiency for Hydrogen Generation. *Inorg. Chem.* **2006**, *45* (23), 9181−9184.
(62) Sampson, M. D.; Nguyen, A. D.; Grice, K. A.; Moore, C. E.; Rheingold, A. L.; Kubiak, C. P. Manganese Catalysts with Bulky Bipyridine Ligands for the Electrocatalytic Reduction of Carbon Dioxide: Eliminating Dimerization and Altering Catalysis. *J. Am. Chem. Soc.* **2014**, *136* (14), 5460−5471.
(63) Ngo, K. T.; McKinnon, M.; Mahanti, B.; Narayanan, R.; Grills, D. C.; Ertem, M. Z.; Rochford, J. Turning on the Protonation-First Pathway for Electrocatalytic CO2 Reduction by Manganese Bipyridyl Tricarbonyl Complexes. *J. Am. Chem. Soc.* **2017**, *139* (7), 2604−2618.
(64) Savéant, J. M.; Vianello, E. Potential-Sweep Chronoamperometry Theory of Kinetic Currents in the Case of a First Order Chemical Reaction Preceding the Electron-Transfer Process. *Electrochim. Acta* **1963**, *8* (12), 905−923.
(65) Talukdar, K.; Issa, A.; Jurss, J. W. Synthesis of a Redox-Active NNP-Type Pincer Ligand and Its Application to Electrocatalytic CO_2 Reduction with First-Row Transition Metal Complexes. *Front. Chem.* **2019**, *7*. DOI: 10.3389/fchem.2019.00330.
(66) Lee, G. R.; Maher, J. M.; Cooper, N. J. Reductive Disproportionation of Carbon Dioxide by Dianionic Carbonylmetalates of the Transition Metals. *J. Am. Chem. Soc.* **1987**, *109* (10), 2956−2962.
(67) Ratliff, K. S.; Lentz, R. E.; Kubiak, C. P. Carbon Dioxide Chemistry of the Trinuclear Complex [Ni3(.Mu.3-CNMe)(.Mu.3-I)(Dppm)3][PF6]. Electrocatalytic Reduction of Carbon Dioxide. *Organometallics* **1992**, *11* (6), 1986−1988.
(68) Simón-Manso, E.; Kubiak, C. P. Dinuclear Nickel Complexes as Catalysts for Electrochemical Reduction of Carbon Dioxide. *Organometallics* **2005**, *24* (1), 96−102.
(69) Machan, C. W.; Chabolla, S. A.; Yin, J.; Gilson, M. K.; Tezcan, F. A.; Kubiak, C. P. Supramolecular Assembly Promotes the Electrocatalytic Reduction of Carbon Dioxide by Re(I) Bipyridine Catalysts at a Lower Overpotential. *J. Am. Chem. Soc.* **2014**, *136* (41), 14598−14607.
(70) Lee, K. J.; McCarthy, B. D.; Dempsey, J. L. On Decomposition, Degradation, and Voltammetric Deviation: The Electrochemist's Field Guide to Identifying Precatalyst Transformation. *Chem. Soc. Rev.* **2019**, *48* (11), 2927−2945.
(71) Chapovetsky, A.; Welborn, M.; Luna, J. M.; Haiges, R.; Miller, T. F.; Marinescu, S. C. Pendant Hydrogen-Bond Donors in Cobalt Catalysts Independently Enhance CO2 Reduction. *ACS Cent. Sci.* **2018**, *4* (3), 397−404.

https://dx.doi.org/10.1021/acs.inorgchem.0c00154
Inorg. Chem. XXXX, XXX, XXX−XXX

(72) Cargill Thompson, A. M. W.; Bardwell, D. A.; Jeffery, J. C.; Ward, M. D. Complexes of the Terdentate N-Donor Ligand 6-(2-Aminophenyl)-2,2′-Bipyridine (L): Crystal Structures of Mononuclear [ZnL2][PF6]2 and Tetranuclear [{CuL(MeCN)}4(M4-PO4)][PF6]5 Containing an Unusual M4-Bridging Phosphate Ion. *Inorg. Chim. Acta* **1998**, *267* (2), 239−247.
(73) Hevia, E.; Pérez, J.; Riera, V.; Miguel, D. New Octahedral Rhenium(I) Tricarbonyl Amido Complexes. *Organometallics* **2002**, *21* (9), 1966−1974.
(74) Machan, C. W.; Kubiak, C. P. Electrocatalytic Reduction of Carbon Dioxide with Mn(Terpyridine) Carbonyl Complexes. *Dalton Trans.* **2016**, *45* (43), 17179−17186.
(75) Sung, S.; Li, X.; Wolf, L. M.; Meeder, J. R.; Bhuvanesh, N. S.; Grice, K. A.; Panetier, J. A.; Nippe, M. Synergistic Effects of Imidazolium-Functionalization on Fac-Mn(CO)3 Bipyridine Catalyst Platforms for Electrocatalytic Carbon Dioxide Reduction. *J. Am. Chem. Soc.* **2019**, *141* (16), 6569−6582.
(76) Grills, D. C.; Matsubara, Y.; Kuwahara, Y.; Golisz, S. R.; Kurtz, D. A.; Mello, B. A. Electrocatalytic CO2 Reduction with a Homogeneous Catalyst in Ionic Liquid: High Catalytic Activity at Low Overpotential. *J. Phys. Chem. Lett.* **2014**, *5* (11), 2033−2038.
(77) Nichols, E. M.; Derrick, J. S.; Nistanaki, S. K.; Smith, P. T.; Chang, C. J. Positional Effects of Second-Sphere Amide Pendants on Electrochemical CO2 Reduction Catalyzed by Iron Porphyrins. *Chem. Sci.* **2018**, *9* (11), 2952−2960.
(78) Roell, S. A.; Schrage, B. R.; Ziegler, C. J.; White, T. A. Isolating Substituent Effects in Re(I)-Phenanthroline Electrocatalysts for CO2 Reduction. *Inorg. Chim. Acta* **2020**, *503*, 119397.

https://dx.doi.org/10.1021/acs.inorgchem.0c00154
Inorg. Chem. XXXX, XXX, XXX−XXX